Synthesis of micro and nanostructured MnO_2 and their comparative study in lithium battery

A. Pendashteh, M. F. Mousavi, M. A. Kiani, S. H. Kazemi & M. S. Rahmanifar

Journal of the Iranian Chemical Society

ISSN 1735-207X
Volume 9
Number 3

J IRAN CHEM SOC (2012) 9:389-395
DOI 10.1007/s13738-011-0049-0

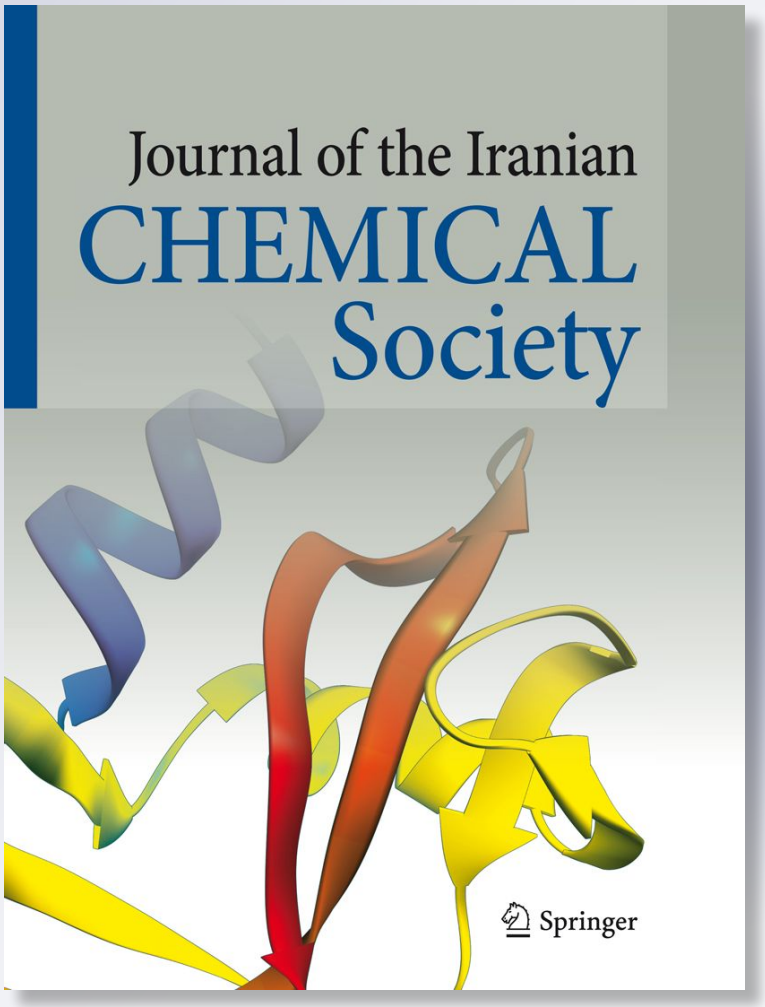

Springer

J IRAN CHEM SOC (2012) 9:389–395
DOI 10.1007/s13738-011-0049-0

ORIGINAL PAPER

Synthesis of micro and nanostructured MnO_2 and their comparative study in lithium battery

A. Pendashteh · M. F. Mousavi · M. A. Kiani · S. H. Kazemi · M. S. Rahmanifar

Received: 14 March 2011 / Accepted: 23 October 2011 / Published online: 5 January 2012

Abstract Micro and nanostructured γ-MnO_2 are synthesized to investigate the size effect of cathode active materials in battery performance. $MnSO_4$ and $(NH_4)_2S_2O_8$ were used as starting materials to prepare micro and nanostructured samples in the presence of stirring and ultrasonic irradiation, respectively. Structure optimization is done by changing values for temperature and manganese sulphate concentration. The MnO_2 micro and nanoparticles are characterized by scanning electron microscopy and X-ray diffraction (XRD). The XRD results reveal that only γ-MnO_2 is formed under the reaction conditions. Under the optimized conditions, manganese dioxide nanoparticles, with an average particle size of 56 nm, are obtained. Both micro and nanostructured MnO_2 is used as the cathode active material in Li/MnO_2 battery. Discharge profiles of stirrer-based cathode material (micro) and ultrasonic instrument-based one (nano) compared with each other in constant discharge currents of 50 and 100 mA g^{-1}. The results demonstrated that nanosized materials show higher specific capacities and energies. Electrochemical impedance spectroscopy is used to investigate the size effect of cathode material on battery resistance and the results show a copious decrease in total resistance.

A. Pendashteh · M. F. Mousavi (✉) · M. A. Kiani
Department of Chemistry, Tarbiat Modares University, P.O. Box 14115-175, Tehran, Iran
e-mail: mfmousavi@yahoo.com; mousavim@modares.ac.ir

S. H. Kazemi
Department of Chemistry, Institute for Advanced studies in Basic Sciences, Zanjan, Iran

M. S. Rahmanifar
Faculty of Basic Sciences, Shahed University, Tehran, Iran

Keywords Lithium battery · Nanostructure · Manganese dioxide · Ultrasonication

Introduction

Among different types of lithium batteries, the primary lithium/manganese dioxide cell was one of the first Li cells to be commercialized. The advantageous features of these cells include high nominal voltage (3 V), high specific energy (230 Wh kg^{-1}), high energy density (535 Wh L^{-1}), and operation over a wide temperature range, superior shelf life, and low cost. Li/MnO_2 primary battery as a high energy density, high drain power source uses heat-treated manganese dioxide (HTMD), a defect pyrolusite structure material as the cathode active material. Actually, γ-MnO_2, which is the most promise candidate among the large variety of manganese oxides for use as positive electrode in non-aqueous batteries, requires a dehydration process above 300 °C [1].

Nanostructures have received steadily growing interest not only for their fundamental scientific significance but also for their many technological applications. These structures have been used extensively in various kinds of energy storage systems [2–4]. Electrochemical properties of a material are extremely affected by the morphology and surface area of the electrode particles. Electrochemical performance of many materials has been improved significantly because of size effect of nanostructured active materials in the electrode [5–10]. Nanostructured materials employed in electrodes decrease solid-state diffusion path length and thereby exhibit better electrochemical performance as expected.

Among a variety of physicochemical methods, including hydrothermal [11], sol-gel [12], electrochemical methods [13] and others, the sonochemical methods have been

shown to be very promising in the preparation of a variety of nanomaterials [14–18]. The success of sonochemistry in creating nanostructured materials principally originates from acoustic cavitation; the formation, growth, and implosive collapse of bubbles in a liquid which causes intense local heating (5,000 °C), pressure (1,800 atm), and cooling rates greater than 10^{10} K s^{-1} [19].

Extensive interests have been focused on developing MnO_2 nanostructures and significant progress has been reported [20–31]. Manganese dioxide can form different types of polymorphs, such as α, β, γ, and δ. Among them, especially γ-MnO_2 has good electrochemical performances and is used in battery industries [32–34].

This work extends our previous studies of various electrochemical energy storage systems, such as polyaniline battery [35–41], and lead–acid battery [42]. Herein, we report the synthesis of micro and nanostructured manganese dioxide and some of reaction conditions including reactant concentration and temperature have been optimized. Synthesized samples were used in Li/MnO_2 batteries as cathode active material. The influence of particle size and structure of cathode active material on battery performance for lithium batteries will also be studied and compared.

Experimental

Apparatus

A multiwave ultrasonic generator (Sonicator-3000; Misonix, Inc., Farmingdale, NY, USA), equipped with a converter/transducer and titanium oscillator (horn), 12.5 mm in diameter, operating at 20 kHz with a maximum power output of 600 W, was employed for the ultrasonic irradiation. The power level was adjusted automatically by the ultrasonic generator. Circulating water from a water bath (Optima, Tokyo, Japan) kept the solution temperature constant. An electrical furnace (Paragon E10, USA) was used to dehydrate the synthesized samples. Morphological studies of prepared samples were performed by SEM (Philips XL 30). XRD (Philips X'pert diffractometer) and Cu K_α radiation ($\lambda = 0.15418$ nm) was used to study the phase composition of the prepared samples. Effective surface area of the samples was measured by Brunauer–Emmett–Teller (BET) (BEL Japan, Inc.). The EIS and discharge tests were carried out using Galvanostat/Potentiostat Autolab (PGSTAT30) connected to a PC.

Materials

$MnSO_4 \cdot H_2O$, $(NH_4)_2S_2O_8$ and propylene carbonate (PC) were supplied from MERCK and used without any purification. $LiClO_4$ was purchased from ACROS for preparing the electrolyte and Lithium (from Fluka) was used as anode material. Doubly distilled water was used throughout.

Synthesis of MnO_2 nanoparticles

A two-walled cylindrical glass cell with an interior volume of 300 ml was employed for the synthesis of MnO_2. The redox reaction between manganese sulphate and ammonium peroxydisulphate was adopted for synthesis of γ-MnO_2. 100 mL of $MnSO_4 \cdot H_2O$ and 100 mL of $(NH_4)_2S_2O_8$ solutions with definite concentrations were mixed together in reaction vessel and the solution was sonicated for 1 h. Then the solution was centrifuged at 7,500 rpm for 5 min. A dark brown precipitate was obtained, washed several times with doubly distilled water and dried in an oven at 80 °C for 6 h. The obtained powder was annealed in 350 °C in electrical furnace for 2.5 h to dehydrate and form HTMD [1].

The experiment was also repeated using stirring in the long enough time of 24 h instead of ultrasonication and the resulting precipitate was centrifuged, washed, and dried as described above.

Characterization

The crystalline phases of the synthesized samples were characterized by X-ray diffraction (XRD) using Cu K_α radiation ($\lambda = 0.15418$ nm). Morphological studies of synthesized samples were performed by scanning electron microscopy, SEM. The BET method [43] was used to measure effective surface area by calculating the amount of absorption/desorption of N_2 gas in a sample.

Electrode fabrication and electrochemical measurements

The positive electrode was fabricated by mixing of the synthesized MnO_2 as the cathode active material, activated carbon (Merck), and polytetrafluoroethylene (PTFE) (60% water based solution from SUTECH, Iran) as binder with a weight ratio of 85:10:5. The resultant slurry was coated onto a nickel plate (1 cm in diameter), pressed under a pressure of 100 kg cm^{-2} and then dried in the oven at 120 °C for 24 h. Cells were composed by stacking cathode against a Li anode, separated by polypropylene separator (Celgard 3401) soaked in electrolyte (1 M $LiClO_4$ in PC). The schematic diagram of the Teflon cell used in the experiments is shown in Fig. 1. Because of the high reactivity of metallic lithium toward atmospheric oxygen, cell assembly and all of the electrochemical tests were performed in an argon atmospheric glove box.

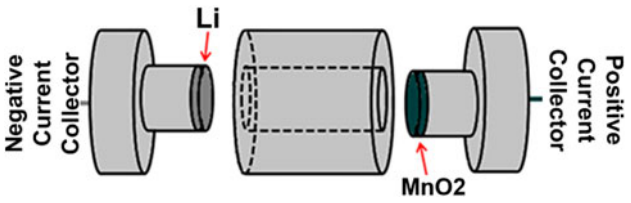

Fig. 1 Schematic diagram of the Teflon cell used in electrochemical experiments

EIS was carried out by applying an ac signal with amplitude of 5 mV at the frequency varying from 100 kHz to 100 mHz at an open circuit voltage (OCV). Data analysis was done based on CNLS method of Boukamp using Zview2 software (Scribner Associates), using an appropriate equivalent circuit described in the text.

The discharge experiments were examined in constant current densities, 50 and 100 mA g^{-1} in the low cut-off voltage of 1.5 V versus Li at 25 °C.

Results and discussion

X-ray studies

Successful synthesis of manganese dioxide was demonstrated by XRD of the prepared samples in all designed conditions. Figure 2a shows the XRD spectrum of the sample prepared by using stirrer. As it can be demonstrated from this spectrum, product of the reaction is $Mn(OOH)_2$ (JCPS card no. 17-0510), a mixture of different manganese oxides with the oxidation states of 2+ and 4+. The exact formula of the product is $Mn^{4+}_{(1-x)}\ Mn^{2+}_{x}O_{(2-2x)}(OH)_{2x}$ when $x = 0.06$–0.07. Manganese content with the oxidation state of 2+ reveals that despite assigning the long enough time (24 h) for reaction to be completed, the oxidant (ammonium peroxydisulphate) could not complete the oxidation of whole manganese content. But irradiating the solution by ultrasonic wave completed the oxidation in a short time of 1 h and resulted the MnO_2 as the only product. It has been demonstrated that ultrasonic irradiation can prompt and complete the oxidation process by hydroxyl radical generation [15]. The oxidation proceeds in the presence of ultrasonication as follows:

$$MnSO_4 \cdot H_2O + (NH_4S_2O_8 + H_2O) \xrightarrow{)))} MnO_2 + (NH_4)_2SO_4 + 2H_2SO_4$$

The X-ray powder diffraction spectrum of nanostructured γ-MnO_2 is shown in Fig. 2b. As it can be seen from XRD spectra, micro-sized samples have clear and sharp peaks which indicate that γ-MnO_2 have big crystallite size unlike

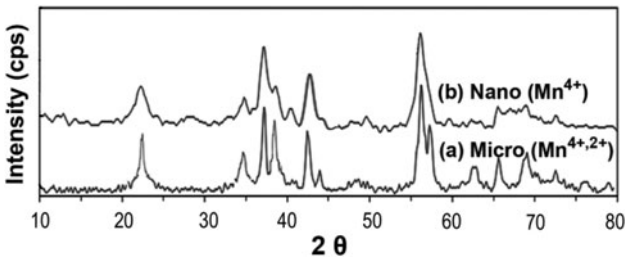

Fig. 2 X-ray powder diffraction pattern for *a* sample prepared in the presence of stirrer (micro), *b* nanostructured γ-MnO_2 in the presence of sonicator

nanosized sample with broader peaks showing the small size of particles.

SEM studies

Figure 3 shows SEM images of micro and nanostructures of γ-MnO_2, synthesized by using stirrer and sonicator, respectively. Figure 3a and b are concerned to the samples, prepared through a simple chemical oxidation using stirrer during the reaction in 50, and 60 °C, respectively. It can be seen from both images that the synthesized particles are aggregated and do not have a definite morphology. We also investigated the effects of manganese sulphate concentration (0.05, 0.1, and 0.2 M) and temperature (40, 50, and 60 °C) on the particle size, and morphology of the prepared manganese dioxide. In previous works, it has been found that the applied ultrasonic wave determines the particle size. Increasing the ultrasonic wave amplitude decreases the rate of particle growth [15]. Therefore, in this work, we have used constant sonication wave amplitude of about 84 μm. The synthesis efficiency at the temperature of 40 °C was too low that the amount of prepared samples was not adequate to be characterized by SEM. Temperatures higher than 60 °C was not investigated because of high vaporization which yields significant concentration changes. Figure 3c, d, and e shows the SEM images of samples synthesized at temperature of 50 °C, but in different concentrations of manganese sulphate of 0.05, 0.1, and 0.2 M, respectively. As it can be observed from these images, size of MnO_2 particles has been reduced by increase in $MnSO_4$ concentration. Furthermore, the increase in $MnSO_4$ concentration has led to change in morphology of prepared samples. Low concentration (0.05 M) leads to the formation of rice-shape particles (Fig. 3c). The prepared nanoparticles in this situation did not grow a lot in length, probably due to the effect of ultrasonication. As the concentration of $MnSO_4$ is raised, the morphology of the synthesized particles changed from rice-shape to globular nanoparticles (Fig. 3d, e). As it can be seen in Fig. 3e, increasing $MnSO_4$ concentration to

0.2 M led to formation of MnO_2 nanoparticles with an average size of 65 nm (57–90 nm). This decrease in size is attributed to more nucleation centres in high concentration of $MnSO_4$, which prevents the nucleation growth process to proceed and therefore leads to smaller particles in size. Figure 3f shows the SEM image of the sample which was synthesized at 60 °C and in $MnSO_4$ concentration of 0.2 M while ultrasonication was applied during the reaction. An increase in temperature reaction from 50 to 60 °C caused a change in solution color from light brown to dark brown, which clearly shows the increase in reaction rate in high temperatures. Figure 3e shows a more compact assemblies or aggregates than those in Fig. 3f, which may be attributed to the partial expansion of nano-MnO_2 aggregates caused by increasing the temperature from 50 to 60 °C. This leads to an increase in the specific surface area of these assemblies. Therefore, the synthesis condition of the sample shown in Fig. 3f was considered as optimized to preparation of the most uniform morphology and the largest specific surface area (20.80 $m^2\ g^{-1}$). Thus, all of the electrochemical tests done to investigate the use of nanoparticles as the cathode material of Li/MnO_2 battery were performed by using the samples synthesized in condition of using sonicator, 0.2 M $MnSO_4$, and 60 °C.

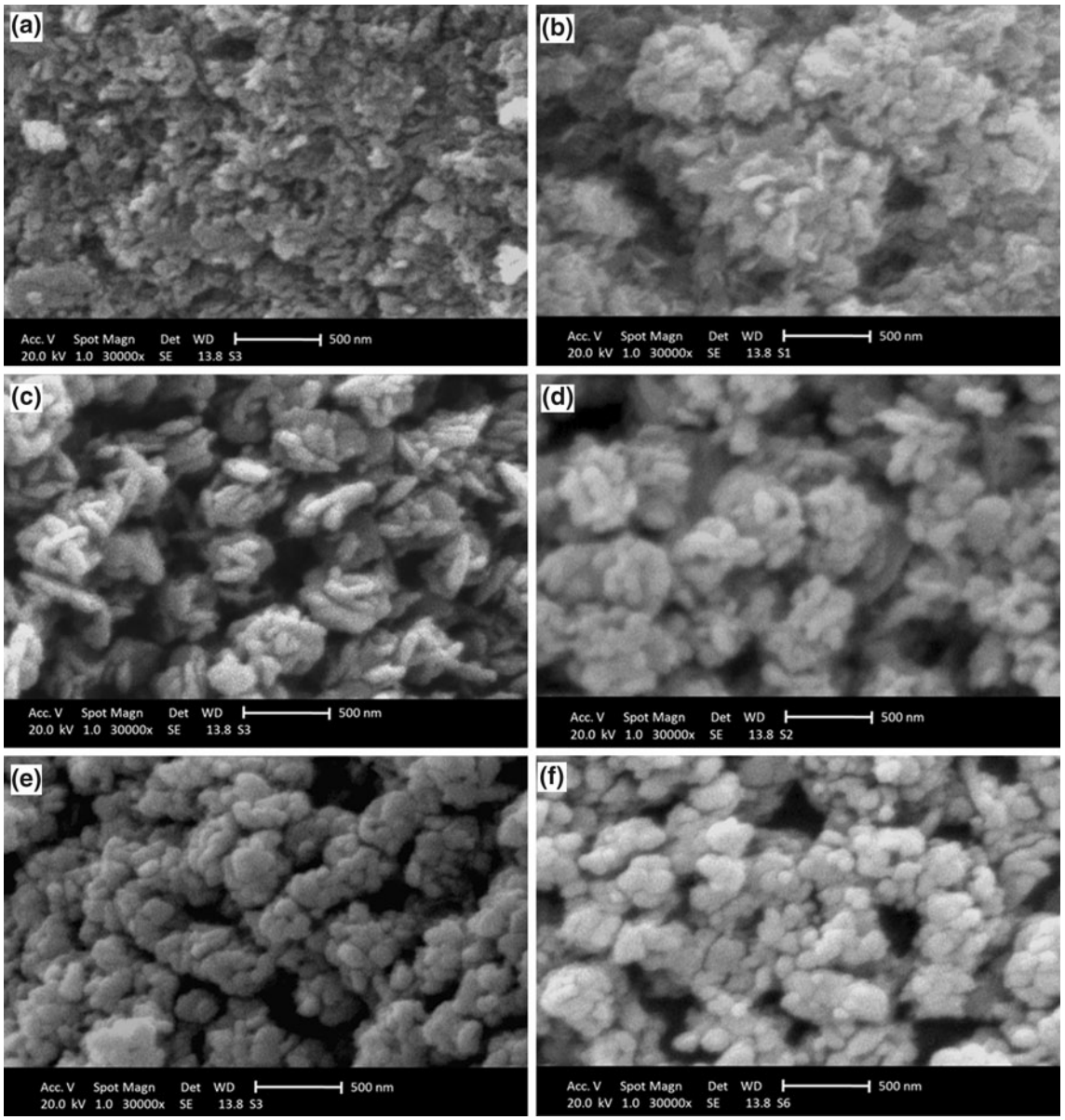

Fig. 3 SEM micrographs of micro and nanostructured γ-MnO_2 synthesized in the presence of stirrer and sonicator, respectively. **a** stirrer, 0.1 M $MnSO_4$, 50 °C, **b** stirrer, 0.1 M $MnSO_4$, 60 °C, **c** sonicator, 0.05 M $MnSO_4$, 50 °C, **d** sonicator, 0.1 M $MnSO_4$, 50 °C, **e** sonicator, 0.2 M $MnSO_4$, 50 °C, **f** sonicator, 0.2 M $MnSO_4$, 60 °C

Porosity measurements

BET was used to measure and compare the effective surface area of prepared microstructured and nanostructured γ-MnO_2. As expected, BET measurements showed larger effective reactive surface area for nanostructured MnO_2 against microstructured one. According to these measurements, specific surface area of micro-synthesized sample is 14.63 m^2 g^{-1}; while that for nanostructure sample synthesized in 50 °C is 17.20 and 20.80 m^2 g^{-1} for the sample synthesized in 60 °C.

Electrochemical studies

Electrochemical impedance measurement in a battery reflects a combined effect of the impedances of negative electrode, electrolyte, and positive electrode and is a powerful method for analysis of internal battery resistance. Typical Nyquist plot of synthesized γ-MnO_2 with micro and nanostructure at OCV are shown in Fig. 4. The spectra display two arcs, one in high-frequency region which is related to the Li-ion migration resistance through the solid electrolyte interface (SEI) film (R_1 coupled with SEI film capacitance), and the second arc in the medium-frequency, corresponds to charge transfer resistance coupled with double layer capacitance [44]. The inset in Fig. 4 depicts the equivalent circuit used to fit experimental data. The parameters of impedance spectra in Fig. 4 were fitted by Zview software. The results are listed in Table 1. In a two-electrode Li/cathode configuration, the contributions of the electrolyte and lithium electrode to the EIS are believed to be constant due to a result of the instant stripping of lithium, which remains the surface of lithium constantly fresh [44]. Therefore, all of the variations in the EIS by changing the cathode material structure can be intrinsically attributed to the structure. The EIS results show that the total resistance is decreased from 131.91 to 88.54 Ω cm^2 as the MnO_2 structure changed from micro to nano. It is obvious that using nanosized material declined the charge transfer resistance, which can be attributed to the decreased diffusion path length due to the presence of small particles in the cathode layer.

Discharge studies

Figure 5a shows the discharge profiles of γ-MnO_2, micro and nanostructures in a constant discharge current density of 50 mA g^{-1}. As it can be seen, the cell with microstructured materials showed a discharge capacity of about 171.26 mAh g^{-1} and the one with nanostructures showed a capacity equal to 213.48 mAh g^{-1} which shows about 25% improvement. In Fig. 5b, it has been shown that the discharge capacity of micro and nanostructure cathode

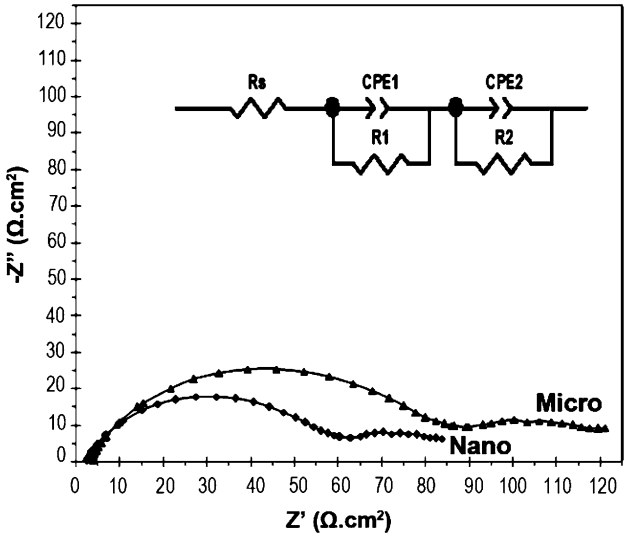

Fig. 4 Comparison of Nyquist plots of micro and nanostructured γ-MnO_2 (MnO_2/Li system, 1 M $LiClO_4$ in PC, at OCV). The *inset* shows the corresponding equivalent circuit used to fit the experimental data

Table 1 Impedance parameters of equivalent circuit used to fit the experimental data

MnO_2	Resistance (Ω cm^2)		
	R_s	R_1	R_2
Micro	3.39	74.20	54.32
Nano	2.37	37.22	48.95

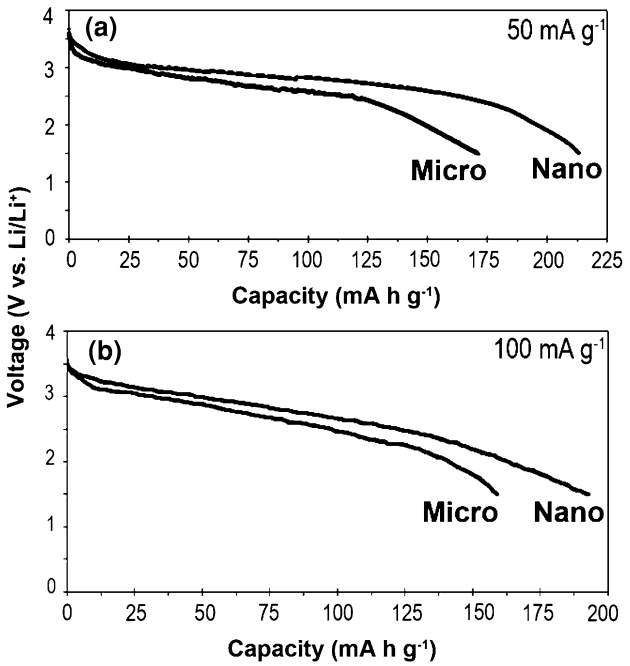

Fig. 5 Comparison of discharge profile of micro and nanostructured γ-MnO_2, at two different current discharge, **a** 50 mA $g^{-1}$and **b** 100 mA g^{-1}

Table 2 Comparison of the current study with some of the investigated systems before

System	Particle size (nm)	Electrolyte	Discharge current (mA g^{-1})	Voltage range (V)	Capacity (mAh g^{-1})	Reference
γ-MnO_2 (bulky)/Li	–	LiPF6-DMC/EC	20	4.0–2.0	181	Lee et al. [46]
α-MnO_2 nanorods/Li	10	LiPF6-DMC/EC	50	3.8–1.5	206.7	Wang et al. [47]
γ-MnO_2 nanorods/Li	20–100	_	50	3.8–1.5	210	Cheng et al. [48]
MnO_2 nanowires/Li	50–100	LiPF6-DMC/EC	150	3.9–2.0	160	Kim et al. [49]
MnO_2 nanowires/Li	50–100	LiPF6-DMC/EC	300	3.9–2.0	150	Kim et al. [49]
Current study	56 (avg.)	$LiClO_4$-PC	50 (100)	3.4–1.5	213.48 (193.02)	–

material is 158.94 and 193.02 mAh g^{-1} at the constant discharge current of 100 mA g^{-1} (about 22% capacity improvement). As seen from discharge profiles in both currents, using nanostructured MnO_2 as cathode material rendered higher average voltage, which it yields higher specific energy. Specific energy (SE) of the battery systems calculated from the following equation:

$$\left[\mathrm{SE} = \frac{IVt}{2M \times 3{,}600}\right] \quad (1)$$

where I is the discharge current density, V is the average voltage, t is the discharge time and M is the amount of active materials in the electrode. In discharge current of 50 mA g^{-1}, the value of specific energy for nanostructured material is 254.41 Wh kg^{-1}; while for microstructured one is 195.91 Wh kg^{-1}. As seen, there is 58.5 Wh kg^{-1} improvement in specific energy by using nanostructured active materiel. It can be seen from discharge profiles that the discharge capacity for nanostructure material showed higher values compared to that of bulk γ-MnO_2. The specific capacity increase in the nanoparticles can be attributed to their small particle size which causes an increase in the active surface area. The increase in the specific surface area, increases the efficiency of the electrochemical insertion of the Li^+ ions into the structure of MnO_2. The nanoparticles have enhanced reactivity due to the increase in surface area. Furthermore, going to the nanosized materials decrease the solid-state diffusion path lengths. All of these lead to an improvement in electrochemical behavior. The discharge capacity at high rate is directly related to the active surface area of the electrodes and thus to the current density [45]. The effective current density (current density per reactive surface area) decreases as the surface area increases. Therefore, the higher surface area of nanostructure cathode material lowers the discharge current density and thereby increases its discharge capacity. According to a literature survey, some of the investigated systems by others listed in Table 2. Capacity values of the current study demonstrate the size effect on battery performance and have a good accordance with reported data of nanostructured MnO_2 and are much higher than that of the related bulk materials.

Conclusion

Nanostructured manganese dioxide was synthesized in the presence of ultrasonic radiation, which facilitated oxidation of manganese sulphate with ammonium peroxydisulphate as an oxidant. The structure of the micro and nanoparticles were characterized by XRD and SEM. The prepared MnO_2 nanoparticles were used as cathode active material in Li/MnO_2 primary cell. Capacities compared to capacities of those cells with the micro-sized cathode material prepared by using stirrer. It is demonstrated that using nanoparticles showed higher capacities of 213.48 and 193.02 mAh g^{-1} at discharge current of 50 and 100 mA g^{-1}, respectively. Electrochemical impedance spectra demonstrated that electrochemical reaction activity of the electrode material with synthesized nanostructure is dramatically improved and the total resistance of the battery is decreased.

Acknowledgments We gratefully acknowledge the Tarbiat Modares University Research Council for financial support of this work.

References

1. W. Bowden, T. Bofinger, F. Zhang, N. Iltchev, R. Sirotina, Y. Paik, J. Power Sources **165**, 609 (2007)
2. Kh. Ghanbari, M.F. Mousavi, M. Shamsipur, Electrochim. Acta. **52**, 1514 (2006)
3. S. Ghasemi, M.F. Mousavi, H. Karami, M. Shamsipur, S.H. Kazemi, Electrochim. Acta. **52**, 1596 (2006)
4. H.R. Ghenaatian, M.F. Mousavi, S.H. Kazemi, M. Shamsipur, Syn. Met. **159**, 1717 (2009)
5. T. Doi, Y. Iriyama, T. Abe, Z. Ogumi, Chem. Mat. **17**, 1580 (2005)
6. H. Li, L. Shi, Q. Wang, L. Chen, X. Huang, Solid State Ionics **148**, 247 (2002)
7. S.S. Zhang, M.S. Ding, K. Xu, J. Allen, T.R. Jow, Electrochem. Solid-State Lett. **4**, A206 (2001)
8. X. Wu, H. Li, L. Chen, X. Huang, Solid State Ionics **149**, 185 (2002)
9. H. Li, L.H. Shi, W. Lu, X.J. Huang, L.Q. Chen, J. Electrochem. Soc. **148**, A915 (2001)
10. Kh. Ghanbari, S.Z. Bathaie, M.F. Mousavi, Biosen. Bioelectron. **23**, 1825 (2008)
11. Q.H. Zhang, S. Sun, S. Li, H. Jiang, J.G. Yu, Chem. Eng. Sci. **62**, 4869 (2007)
12. M. Sugantha, P.A. Ramakrishnan, A.M. Hermann, C.P. Warmsingh, D.S. Ginley, Int. J. Hydrogen Energy **28**, 597 (2003)

13. M. Wu, L. Zhang, J. Gao, C. Xiao, D. Wang, A. Chen, S. Zhang, J. Electroanal. Chem. **613**, 125 (2008)
14. M.A. Kiani, M.F. Mousavi, S. Ghasemi, J. Power Sources **195**, 5794 (2010)
15. S. Ghasemi, M.F. Mousavi, M. Shamsipur, H. Karami, Ultrason. Sonochem. **15**, 448 (2008)
16. A. Zolfaghari, F. Ataherian, M. Ghaemi, A. Gholami, Electrochim. Acta. **52**, 2806 (2007)
17. K.H. Kim, K.B. Kim, Ultrason. Sonochem. **15**, 1019 (2008)
18. E. Ohayan, A. Gedanken, Ultrason. Sonochem. **17**, 173 (2010)
19. K.S. Suslick, *Sonochemistry, Kirk-Othmer Encyclopedia of Chemical Technology, 4th edn., vol. 26* (Wiley, New York, 1998), pp. 517–541
20. L. Yuan, Z. Li, J. Sun, K. Zhang, Y. Zhou, Mater. Lett. **57**, 1945 (2003)
21. M.S. Wu, Appl. Phys. Lett. **87**, 153102 (2005)
22. M.S. Wu, J.T. Lee, Y.Y. Wang, C.C. Wan, J. Phys. Chem. B **108**, 16331 (2004)
23. L. Li, Y. Pan, L. Chen, G. Li, J. Solid State Chem. **180**, 2896 (2007)
24. F.Y. Cheng, J. Chen, X.L. Gou, P.W. Shen, Adv. Mater. **17**, 2753 (2005)
25. F.Y. Cheng, J.Z. Zhao, W.E. Song, C.S. Li, H. Ma, J. Chen, P.W. Shen, Inorg. Chem. **45**, 2038 (2006)
26. V. Subramanian, H.W. Zhu, R. Vajtai, P.M. Ajayan, B.Q. Wei, J. Phys. Chem. B **109**, 20207 (2005)
27. Z.Y. Yuan, Z. Zhang, G. Du, T.Z. Ren, B.L. Su, Chem. Phys. Lett. **378**, 349 (2003)
28. C.Z. Wu, Y. Xie, D. Wang, J. Yang, T.W. Li, J. Phys. Chem. B **107**, 13583 (2003)
29. Y. Xiong, Y. Xie, Z. Li, C. Wu, Chem. Eur. J. **9**, 1645 (2003)
30. X. Wang, Y.D. Li, Chem. Commun. **764** (2002)
31. X. Wang, Y.D. Li, J. Am. Chem. Soc. **124**, 2880 (2002)
32. B. Ammundsen, J. Paulsen, Adv. Mater. **13**, 943 (2001)
33. M.S. Whittingham, Chem. Rev. **104**, 4271 (2004)
34. M.M. Thackeray, Prog. Solid State Chem. **25**, 1 (1997)
35. M.S. Rahmanifar, M.F. Mousavi, M. Shamsipur, J. Power Sources **110**, 229 (2002)
36. H. Karami, M.F. Mousavi, M. Shamsipur, J. Power Sources **117**, 255 (2003)
37. H. Karami, M.F. Mousavi, M. Shamsipur, J. Power Sources **124**, 303 (2003)
38. M.S. Rahmanifar, M.F. Mousavi, M. Shamsipur, M. Ghaemi, J. Power Sources **132**, 296 (2004)
39. M.S. Rahmanifar, M.F. Mousavi, M. Shamsipur, H. Heli, Syn. Met. **155**, 480 (2005)
40. H. Karami, M.F. Mousavi, M. Shamsipur, S. Riahi, J. Power Sources **154**, 298 (2006)
41. Kh. Ghanbari, M.F. Mousavi, M. Shamsipur, H. Karami, J. Power Sources **170**, 513 (2007)
42. H. Karami, M. Shamsipur, S. Ghasemi, M.F. Mousavi, J. Power Sources **164**, 896 (2007)
43. S. Brunauer, P.H. Emmett, E. Teller, J. Am. Chem. Soc. **60**, 309 (1938)
44. S.S. Zhang, K. Xu, T.R. Jow, Electrochim. Acta. **51**, 1636 (2006)
45. J. Drews, R. Wolf, G. Fehrmann, R. Staub, J. Power Sources **65**, 129 (1997)
46. J. Lee, J.M. Lee, S. Yoon, S.O. Kim, J.S. Sohn, K.I. Rhee, H.J. Sohn, J. Power Sources **183**, 325 (2008)
47. H. Wang, Z. Lu, D. Qian, S. Fang, J. Zhang, J. Alloys Compd. **466**, 250 (2008)
48. F. Cheng, J. Zhao, W. Song, C. Li, H. Ma, J. Chen, P. Shen, Inorg. Chem. **45**, 2038 (2006)
49. J.H. Kim, T. Ayalasomayajula, V. Gona, D. Choi, J. Power Sources **183**, 366 (2008)